

DAMAGE PROGRESSION IN LAMINATES UNDER
IN-PLANE AND EDGE MOMENT LOADS

by

HUNG-YI LU

Presented to the Faculty of the Graduate School of
The University of Texas at Arlington in Partial Fulfillment
of the Requirements
for the Degree of

MASTER OF SCIENCE IN AEROSPACE ENGINEERING

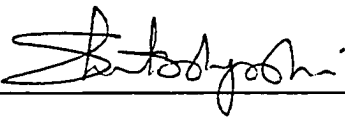
THE UNIVERSITY OF TEXAS AT ARLINGTON

December 1992

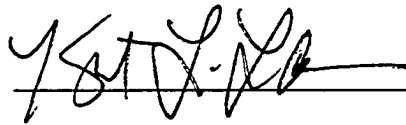
DAMAGE PROGRESSION IN LAMINATES UNDER IN-PLANE AND
EDGE MOMENT LOADS

The members of the Committee approve the masters
thesis of Hung-Yi Lu

Shiv P. Joshi
Supervising Professor



Kent L. Lawrence



Wen S. Chan



ACKNOWLEDGMENTS

I would like to express my appreciation to Dr. S.P. Joshi for his helping me in anything that I need. This thesis could not have been written without his help. I would also like to thank Dr. W.S. Chan and Dr. K.L. Lawrence for their help in serving my thesis committee. In the meanwhile, I would thank Sandy for her encouraging me during this research work period. Finally I would like to dedicate this paper to my parents for their eternal love to me.

November 30, 1992

ABSTRACT

DAMAGE PROGRESSION IN LAMINATES UNDER IN-PLANE AND EDGE MOMENT LOADS

Publication No. _____

Hung-Yi Lu, M.S.

The University of Texas at Arlington, 1992

Supervising Professor: Shiv P. Joshi

Damage progression in laminates with in-plane loads and edge moments is investigated herein analytically. Simple-supported laminated composite columns subjected to off-center compressive loads are analyzed. They undergo large displacement while strains remain small when subjected to off-center compressive load. The damage initiates before the column buckles. The stress gradients appear along the length of the column because of the large displacement. Wolfe used these columns in experimental study of damage progression in a gradient stress field. The same composite laminate column geometry and lay-ups are analyzed using the finite element method which incorporates the two phases continuum damage model. The geometric nonlinearity due to large displacements is implemented in an approximate way in the finite element procedure. The damage initiation load predictions compare favourably with the experimental results. The prediction of plies and the planer location within the ply where damage initiates also matches with the experimental observations.

TABLE OF CONTENTS

ACKNOWLEDGMENTS.....	iii
ABSTRACT	iv
LIST OF FIGURES	vii
LIST OF TABLES.....	ix
1. INTRODUCTION	1
2. HISTORICAL APPROACH SUMMARY.....	3
3. DAMAGE EVOLUTION THEORY	6
3.1 Two Phases Continuum Model	6
3.2 Two Phases Constitutive Model	7
3.3 Damage Evolution Model.....	8
3.4 Laminate Constitutive Behavior.....	9
3.5 Pre-Ply Failure.....	10
3.6 Post-Ply Failure.....	11
4. MATERIAL PROPERTIES DETERMINATION	13
5. FINITE ELEMENT METHOD MODEL	16
5.1 FEM Formulation.....	16
5.2 The FEM Model.....	19
5.3 FEM Procedure for Large Displacement.....	22
5.4 Damage Evolution Model Implementation.....	25

6. NUMERICAL SIMULATIONS.....	29
7. SUMMARY AND RECOMMENDATIONS	45
REFERENCES	47

LIST OF FIGURES

5.1 Nine Node Isoparametric Element	18
5.2 Configuration of Test Jig	21
5.3 Mesh Generation in Laminate	22
5.4 Equilibrium of a Small Element of a Column under Compressive in-plane Load and Moment	23
5.5 An Approximate Approach in Load Modification due to Large Displacement	24
5.6 Relationship between Lateral Displacement, in-plane Load and Moment on Successive Nodes	25
5.7 Flowchart for Damage Evolution Model Implementation	28
6.1 Experimental and Predicted Load versus Center Deflection for $[45_4^\circ / -45_4^\circ / (0^\circ / 90^\circ)_4]_{2s}$ prior to Damage	33
6.2 Experimental and Predicted Load versus Centerline Strain for $[45_4^\circ / -45_4^\circ / (0^\circ / 90^\circ)_4]_{2s}$ prior to Damage	34
6.3 Experimental and Predicted Load versus Center Deflection for $[\pm 45^\circ / 0^\circ / 90_4^\circ]_{4s}$ prior to Damage	35
6.4 Experimental and Predicted Load versus Centerline Strain for $[\pm 45^\circ / 0^\circ / 90_4^\circ]_{4s}$ prior to Damage	36
6.5 Experimental and Predicted Load versus Center Deflection for $[(45_2^\circ / -45_2^\circ / 0^\circ)_2 / 90_5^\circ]_{2s}$ prior to Damage	37

6.6 Experimental and Predicted Load versus Centerline Strain for

$\left[\left(45_2^\circ / -45_2^\circ / 0^\circ \right)_2 / 90_5^\circ \right]_{2s}$ prior to Damage.....	38
6.7 First Critical Damage in $\left[-45_4^\circ / -45_4^\circ / \left(0^\circ / 90^\circ \right)_4 \right]_{2s}$ Lay-up.....	40
6.8 First Critical Damage in $\left[\pm 45^\circ / 0^\circ / 90_4^\circ \right]_{4s}$ Lay-up.....	41
6.9 First Critical Damage in $\left[\left(45_2^\circ / -45_2^\circ / 0^\circ \right)_2 / 90_5^\circ \right]_{2s}$ Lay-up.....	42
6.10 Subsequent Critical Damage in $\left[-45_4^\circ / -45_4^\circ / \left(0^\circ / 90^\circ \right)_4 \right]_{2s}$ Lay-up.....	43
6.11 Subsequent Critical Damage in $\left[\pm 45^\circ / 0^\circ / 90_4^\circ \right]_{4s}$ Lay-up.....	44

LIST OF TABLES

4.1 Material Constants for As-4/3501-6 Graphite Epoxy	14
4.2 As4/3501-6 Damage Growth Constants.....	15
6.1 Experimental Damage Initiation Loads and Model Predictations	32

CHAPTER 1

INTRODUCTION

Light weight, high stiffness and strength properties of composites have made them superior to the conventional isotropic materials in aerospace industry. These light weight materials can carry loads in preferred directions because of the orthotropic properties of the composite materials. Also the light weight makes them an attractive material to replace some metals in structures. Though composite materials have many advantages compared to traditional isotropic materials, however their full potential is not utilized in current structural design. This is because of complexity involved in designing and analyzing structures composed of composite materials.

Structural components used for aerospace applications are often subjected to compressive loads. As a result, the phenomenon of buckling must be understood. The buckling and postbuckling behavior of composite plates and panels has been studied extensively. Predictions of incipient buckling loads and of postbuckling behavior are complicated by boundary conditions, material coupling, and damage. Models of buckling behavior work relatively well up to the occurrence of damage. However, once damage occurs, the symmetry of the specimen is usually destroyed. As a result, predictions become difficult to make.

The rapidly increasing use of high-strength, high-modulus composite materials in advanced engineering structures has generated a research interest in the damage tolerance and reliability of such materials. The emerging interest in understanding and modeling the process of damage accumulation has gained momentum in recent years. Although significant effort has been spent in this area, this research is still in its infancy.

Advanced composite materials suffer from initiation and growth of microcracks even at low loads. Such growth affects substantially the overall behavior of composite materials under subsequent complex loadings. It is important to understand the behavior of materials containing an acceptable level of damage in order to predicting the remaining life.

The objective of this study is to verify the damage prediction capability of the finite element procedure which incorporates two phases continuum damage constitutive relations. Damage progression in laminates with in-plane loads and edge moments is investigated herein analytically. Simple-supported laminated composite columns subjected to off-center compressive loads are analyzed. They undergo large displacement while strains remain small when subjected to off-center compressive load. The damage initiates before the column buckles. The stress gradients appear along the length of the column because of the large displacement. Wolfe[1] used these columns in experimental study of damage progression in a gradient stress field. The same composite laminate column geometry and lay-ups are analyzed using the finite element method which incorporates the two phases continuum damage model. The geometric nonlinearity due to large displacements is implemented in an approximate way in the finite element procedure. The damage initiation load predictions compare favorably with the experimental results. The prediction of plies and the planer location within the ply where damage initiates also matches with the experimental observations.

Chapter 2 contains a summary of previous work about buckling and post buckling study and the continuum damage approach. A short discussion about different approaches is included. In chapter 3 the two phases continuum damage evolution theory is discussed briefly. Material constants necessary in implementing the continuum damage model are derived for AS4/3501-6 in chapter 4. The finite element model for damage evolution and load modification are discussed in chapter 5. In chapter 6, the theoretical predictions are compared with the experimental results. Damage histories in specimens are also compared. Conclusion and recommendation for further study are also presented in the same chapter.

CHAPTER 2

HISTORICAL APPROACH SUMMARY

Damage evolution behavior has been an important issue in composite laminates. A symmetric evolution of damage in even symmetric laminates subjected to in-plane shear or flexural loads makes the behavior of damaged components complicated. It becomes more complicated to understand the behavior when the damage progression occurs. It is a fact that composite plates still have a good ability to carry loads after the micro structure damage in layers. Therefore, it is important to investigate the whole damage evolution in order to make use of the plate even after an acceptable amount of damage occurs.

Leissa[2] collected 400 references about buckling and post buckling in laminates. He found that composite plates buckles at lower loads when coupling between in-plane loads and bending is involved. Also the damage induced unsymmetry produces more elastic coupling which complicates the process. Mingust, Dugundji and Lagace[3] used rectangular flat laminate plates as a model which the coupling terms, transverse shear, nonlinear strain are included. They employed a Reissner-Mindlin plate theory with Rayleigh-Ritz method to obtain the deformation. This model gives good results compared with the experimental results.

Jensen and Lagace[4] use anisotropic plates with uniaxial compression load under several boundary conditions. They find that coupling complicates the plates behavior and reduces the buckling loads. Also the lateral displacement occurs as bending coupling is produced.

Although by means of the model and some experimental results from the authors mentioned above, satisfactory results can be obtained for a buckling problem, however, a study of the damage evolution during the loading is still in its infancy.

The first application of continuum mechanics to treat microstructure damage is attributed to Kachanov[5]. In this method it is recognized that the exact analysis of a multiply connected domain with numerous microcracks is hopelessly complex. Therefore, the effects of these microcracks on macrophysical response are reflected via one or more internal state variable [6] called damage parameters.

Wolfe[1] employed two dimensional, plane stress eight node finite elements to model composite columns. Damage evolutions was accounted for by setting appropriate element stiffness to zero for in-plane modes. Delamination was modelled by effectively disconnecting affected elements.

Goode[7] implemented the damage growth theory which continually updates the stiffness matrices of individual elements of the finite element method as loads are incrementally applied. The finite element analysis of the structure has the capability to determine local, highly stressed regions of the component where damage accumulation would be expected to be greatest.

A large body of information is available on experimental characterization of damage in advanced composite materials[8,9]. Experimental evidence shows the complexity of damage modes in composite materials. Many investigator have considered the effect of damage development in composite material modeling. Tsai[10] considered various schemes to discount ply properties in the presence of damage. Schapery [11] utilized fracture mechanics concepts for life prediction. The theory has been employed for predicting the behavior of quasi-isotropic random particulate composites such as solid propellant. Laws et al.[12] obtained analytical solutions for effective moduli of elastic composites with distributed cracks. The cracks were aligned in predetermined directions, and the overall crack surface area had a first order effect on the stiffness. Talreja[13] employed vector fields where the direction and magnitude of each vector provided a characterization of damage. Allen et al.[14,15] characterized damage by a set of second order tensor valued internal variables representing

locally averaged measures of specific damage mode. Frantziskonis[16] considered material behavior as composed of two fractions, damaged and undamaged. Joshi and Frantziskonis[17,18] presented further developments and addressed some important issues on the approach introduced in reference[16].

CHAPTER 3

DAMAGE EVOLUTION THEORY

This model includes three parts, a two phases continuum model, the constitutive model for two phases and the damage evolution law.

3.1 Two Phases Continuum Model

Let us consider a small volume element (ΔV) in the material. ΔV_d represents the homogeneously distributed damaged phase of the material. Define σ_{ij}^u and σ_{ij}^d as volume averaged stress tensors of the damaged and undamaged parts of the material. The volume averaged strain tensor of the damaged part and the undamaged part are equal when the effect of diffusion between the two phases is not considered.

$$\varepsilon_{ij} = \varepsilon_{ij}^u = \varepsilon_{ij}^d \quad (3.1)$$

where ε_{ij} , ε_{ij}^u , ε_{ij}^d are damaged strain tensors in the volume element, undamaged part, and damaged part.

Also the volume averaged stress tensor in the macroscopic volume can be written through the stress tensor in constituent phases according to the theory of mixtures.

$$\sigma_{ij} = (1-r)\sigma_{ij}^u + r\sigma_{ij}^d \quad (3.2)$$

where $r = \frac{\Delta V_d}{\Delta V}$

3. 2 Two Phases Constitutive Model

The undamaged phase can be considered as linear and elastic.

$$\sigma_{ij}^u = C_{ijkl}^u \varepsilon_{kl} \quad (3.3)$$

where C_{ijkl}^u is the constitutive tensor. Taking the transversely isotropic material with plane stress into account, we can get

$$\begin{bmatrix} \sigma_{11}^u \\ \sigma_{22}^u \\ \sigma_{12}^u \end{bmatrix} = \begin{bmatrix} Q_{11}^u & Q_{12}^u & 0 \\ Q_{12}^u & Q_{22}^u & 0 \\ 0 & 0 & Q_{66}^u \end{bmatrix} \begin{bmatrix} \varepsilon_{11} \\ \varepsilon_{22} \\ \varepsilon_{33} \end{bmatrix} \quad (3.4)$$

where the subscript 1 and 2 indicate the principal material direction. The coefficient of Q_{ij}^u can be derived from material constants E_{11} , E_{22} , ν_{12} , and G_{12} .

Also the damaged phase is linearly and elastic. The constitutive model in damage phase is

$$\sigma_{ij}^d = C_{ijkl}^d \varepsilon_{kl} \quad (3.5)$$

where $C_{ijkl}^d = \begin{bmatrix} Q_{11}^d & Q_{12}^d & 0 \\ Q_{12}^d & Q_{22}^d & 0 \\ 0 & 0 & Q_{66}^d \end{bmatrix}$

The spherical part of σ_{ij}^{dm} which is the stress tensor of the matrix in the damaged part can be related to the strain tensor by

$$\sigma_{kk}^{dm} = \Lambda \varepsilon_{kk}^{dm} \quad (3.6)$$

where Λ is the bulk modulus of the matrix in the damaged phase.

With the assumptions indicated before, materials constants of the damaged part can be derived as follows.

$$\begin{aligned}
 E_{11}^d &= V_f E_{11}^f \\
 \frac{1}{E_{22}^d} &= \frac{(V_f + 2\nu^f V_m)^2}{V_f E^f} + \frac{V_m}{\Lambda} + \frac{2V_m^2(1 + \nu^f)(1 - 2\nu^f)}{V_f E^f} \\
 \nu_{12}^d &= \nu^f V_f + \frac{1}{2} V_m \\
 G_{12}^d &= 0
 \end{aligned} \tag{3.7}$$

where V_f and V_m are fiber and matrix volume fraction. The superscript f indicates the fiber. All these constants are substituted in the transversely isotropic, plane stress constitutive relation to obtain relations for the damaged phase.

Combining equations(3.2) and equation(3.5), and rewriting the total derivative of the equation, then

$$\dot{\sigma}_{ij} = L_{ijkl} \dot{\varepsilon}_{ij} - T_{ij} \tag{3.8}$$

where

$$L_{ijkl} = (1-r)C_{ijkl}^u + rC_{ijkl}^d \tag{3.9}$$

and

$$T_{ij} = \dot{r}(\sigma_{ij}^u - \sigma_{ij}^d) \tag{3.10}$$

3.3 Damage Evolution Model

In order to relate to the irreversible nature of the damage, only the positive load incremental rate will be considered.

The damage parameter is a function of strain as follows.

$$\dot{r} = \begin{cases} A\dot{\varepsilon}_{11} + B\dot{\varepsilon}_{22} + C\dot{\varepsilon}_{12} & \text{when } \dot{r} > 0 \\ 0 & \text{when } \dot{r} < 0 \end{cases} \quad (3.11)$$

The critical value of r can be found through the quadratic function of strain.

$$r_{cr} = a(\varepsilon_{11}^f)^2 + a_1|\varepsilon_{11}^f\varepsilon_{22}^f| + b(\varepsilon_{22}^f)^2 + c(\varepsilon_{12}^f)^2 \quad (3.12)$$

The equation above is also applicable at pre-failure strain states, the following expressions are obtained for coefficients A , B and C .

$$\begin{aligned} A &= 2a\varepsilon_{11} + a_1\text{sign}|\varepsilon_{11}\varepsilon_{22}|\varepsilon_{22} \\ B &= 2b\varepsilon_{22} + a_1\text{sign}|\varepsilon_{11}\varepsilon_{22}|\varepsilon_{11} \\ C &= 2c\varepsilon_{12} \end{aligned} \quad (3.13)$$

The constants a , b , c and a_1 are obtained from test data, The damage phase growth is only a function of strain and strain rates. Equations are represented in principal material directions. The function sign gives 1 or -1 according to the sign of the argument.

3.4 Laminate Constitutive Behavior

The constitutive tensors C^u , C^d also can be transformed to any arbitrary fiber direction.

$$\begin{aligned} \bar{C}^u &= T^T C^u T \\ \bar{C}^d &= T^T C^d T \end{aligned} \quad (3.14)$$

where T is singular transform matrix.

The laminate constitutive equations are derived from the classical lamination theory.

$$\begin{Bmatrix} N \\ M \end{Bmatrix} = \begin{bmatrix} A & B \\ B & D \end{bmatrix} \begin{bmatrix} \varepsilon^o \\ \kappa^o \end{bmatrix} \quad (3.15)$$

where $[N] = [N_x, N_y, N_{xy}]^T$

$$[M] = [M_x, M_y, M_{xy}]^T$$

and ABD matrix is as follows.

$$\begin{aligned} A_{ij} &= \sum_{k=1}^N \left\{ (1-r_k) [\bar{Q}_{ij}^u]_k + r_k [\bar{Q}_{ij}^d]_k \right\} (z_k - z_{k-1}) \\ B_{ij} &= \frac{1}{2} \sum_{k=1}^N \left\{ (1-r_k) [\bar{Q}_{ij}^u]_k + r_k [\bar{Q}_{ij}^d]_k \right\} (z_k^2 - z_{k-1}^2) \\ D_{ij} &= \frac{1}{3} \sum_{k=1}^N \left\{ (1-r_k) [\bar{Q}_{ij}^u]_k + r_k [\bar{Q}_{ij}^d]_k \right\} (z_k^3 - z_{k-1}^3) \end{aligned} \quad (3.16)$$

The mid plane strains and curvatures are as follows.

$$\begin{aligned} [\varepsilon^o] &= [\varepsilon_x^o, \varepsilon_y^o, \varepsilon_{xy}^o]^T \\ [\kappa] &= [\kappa_x, \kappa_y, \kappa_{xy}]^T \end{aligned} \quad (3.17)$$

When $r_k = 0$, ABD matrix will simplify to the classical form. The strains and curvatures are more accurately when damage parameter in the material involved in classical lamination theory.

3.5 Pre-Ply Failure

Ply failure occurs when the damage parameter r reaches the critical value r_{cr} . The rate of damage growth in each ply is different depending on the stacking sequence and fiber orientation. Since different materials properties are assigned in tension and compression cases, the strains in each ply must be known so that the corresponding parameters can be used in

evaluating damage growth. This is achieved by performing an analysis with $r_k=0$ for all the plies. The parameters obtained in this way are applicable up to a ply failure. As mentioned above, the loading is gradually increased (in small increments). At each load increment, the strain field in each ply is obtained from constitutive relations (equation(3.16)). These strains determine the damage parameter r (equation(3.11)), which in turn modifies the constitutive relations used to obtain the strain. Therefore, strains and the damage parameter are iteratively obtained at each load increment. The k th ply fails when r_k for that ply reaches the critical value.

3.6 Post-Ply Failure

After a ply has failed ($r_k = r_{cr}$), that ply is considered to be consisting of a new material as a result of critical degradation of material properties. Both C^u and C^d are modified to represent the critically failed ply. The elements of the C^u and C^d matrices are redefined according to the identified damage modes at failure. The damage mode identified by comparing the strains in the material directions of the failed ply with respect to failure strains in respective material directions. The failure strains are defined for the same ply without any restrains from the adjacent plies (experimentally obtained failure strains for the orthotropic ply). Two simple failure modes are identified and implemented. The first failure mode implies complete degradation of the matrix but not the complete fiber fracture. In this case, The stiffness (in both u- and d- parts) in the transverse direction and shear stiffness are assigned zero values. Also, the Poisson's ratio (ν_{12}) is assumed to be zero. The value of r keeps increasing beyond r_{cr} for that ply until fiber fracture occurs.

The complete fiber fracture occurs when r reached twice the r_{cr} value. Note that the new evolution law for r is described as

$$r = r_{cr} + a^2 \varepsilon_{11}^2 \quad (3.18)$$

where $a^2 = \frac{r_{cr}}{(\varepsilon_{11}^f)^2}$

This law depends only on the strain in fiber direction and estimates final failure when the strain in fiber direction reaches failure strain for that direction. The other damage mode implies fiber fracture but partial matrix degradation. All the elements of the C^u and C^d matrices are assigned to zeros values except C_{22}^u and C_{22}^d . This implies zero stiffness in fiber directions, no resistance in shear and no Poisson's effect. However, the stiffness decreases continuously in the transverse direction. Again, the value of r keeps increasing beyond r_{cr} for the failed ply until it reaches twice the r_{cr} value, which implies complete matrix degradation. The damage evolution law for the ply failed in this mode is redefined as

$$r = r_{cr} + b^2 \varepsilon_{22}^2 \quad (3.19)$$

where $b^2 = \frac{r_{cr}}{(\varepsilon_{22}^f)^2}$

The stresses are redistributed when a ply fails. As an increment in the damage state, the other layers will establish a new equilibrium state in order to maintain the unstable damage situation. After each ply fails in at least one mode of failures, the laminates are completely failure.

CHAPTER 4

MATERIAL PROPERTIES DETERMINATION

Hercules AS4/3501-6 is used in experiments by Wolfe [1]. The same material is used in the numerical simulation. Table 4.1 presents elastic and strength properties of HERCULES AS4/3501-6 graphite epoxy tape [7]. Three different lay-ups are chosen for numerical simulation. They are same as the one used in Reference [1]. The plies with the same orientation adjacent to each other are group together and treated as a single effective ply with the nominal material constants. Two laminates $[\pm 45^\circ / 0^\circ / 90^\circ]_{4s}$ and $[(45^\circ_2 / -45^\circ_2 / 0^\circ) / 90^\circ]_{2s}$ are chosen in which the initial damage appears in the 90° tension plies. Also $[45^\circ_4 / -45^\circ_4 / (0^\circ / 90^\circ)]_{2s}$ is chosen in which the initial damage comes from the 45° plies in tension side.

The damage parameter r and other damage growth constants a_c, a_t, b_c, b_t and c are determined from uniaxial tension, compression and shear tests. All the constants above can be derived from the stress and strain at the failure point.

The critical values (r_{cr}) for damage parameter and c are derived from simple shear tests[16]. The constitutive relation at failure is

$$\sigma_{ij}^f = (1 - r_{cr}) G_{12}^u \varepsilon_{11}^f \quad (4.1)$$

From the equation(4.1), the damage parameter can be determined with all the shear moduli prior to damage and the shear stress at the failure point. the value of c will be determined by taking the value of r into equation(3.11).

Table 4.1

Material Constants for As-4/3501-6 Graphite Epoxy

$$\begin{aligned}
 E_1^t &= 155.13 \text{ GPa} & \sigma_{11}^f &= 2.17 \text{ GPa} & \varepsilon_{11}^f &= 0.014 \\
 E_1^c &= 120.3 \text{ GPa} & \sigma_{11}^{fc} &= 1.4 \text{ GPa} & \varepsilon_{11}^{fc} &= 0.012 \\
 E_2^t &= 9.65 \text{ GPa} & \sigma_{22}^f &= 53.8 \text{ GPa} & \varepsilon_{22}^f &= 0.0067 \\
 E_2^c &= 12.96 \text{ GPa} & \sigma_{22}^{fc} &= 258.8 \text{ GPa} & \varepsilon_{22}^{fc} &= 0.023 \\
 G_{12} &= 5.86 \text{ GPa} & \sigma_{12}^f &= 80.7 \text{ MPa} & \varepsilon_{12}^f &= 0.02 \\
 \nu_{12}^t &= 0.3 & \nu_{12}^c &= 0.3 & & \\
 \nu_{12}^f &= 0.3 & \nu_{12}^{fc} &= 0.3 & &
 \end{aligned}$$

The value of a_c , a_t , b_c and b_t are derived from failure stress-strain data with uniaxial tension and compression [16]. Four damage growth equations are expressed to solve the rest material constants a_c , a_t , b_c and b_t . All the equations need all the failure strain in fiber direction and transverse direction. The failure strain with an overbar represents failure value in transverse direction. With an iteration method to converge by moving the last term to the left-hand side, all the damage growth constants come from the equations (4.2).

Table 4.2 summaries the material constants derived from AS4/3501-6 graphite epoxy tape experiments.

$$\begin{aligned}
r_{cr} &= a_c (\varepsilon_{11}^{fc})^2 + b_t \left| (\bar{\varepsilon}_{22}^f)^2 \right| + \sqrt{a_c a_t} \varepsilon_{11}^{fc} \bar{\varepsilon}_{22}^f \\
r_{cr} &= a_c (\varepsilon_{11}^{fc})^2 + b_t \left| (\varepsilon_{22}^f)^2 \right| + \sqrt{a_c a_t} \bar{\varepsilon}_{11}^{fc} \varepsilon_{22}^f \\
r_{cr} &= a_t (\varepsilon_{11}^f)^2 + b_c \left| (\bar{\varepsilon}_{22}^{fc})^2 \right| + \sqrt{a_c a_t} \varepsilon_{11}^{fc} \bar{\varepsilon}_{22}^f \\
r_{cr} &= a_c (\bar{\varepsilon}_{11}^f)^2 + b_t \left| (\varepsilon_{22}^{fc})^2 \right| + \sqrt{a_c a_t} \bar{\varepsilon}_{11}^{fc} \varepsilon_{22}^f
\end{aligned} \tag{4.2}$$

Table 4.2

As4/3501-6 Damage Growth Constants

$$a_c = 1048.34 \quad b_c = 555.826$$

$$a_t = 1171.46 \quad b_t = 6919.9$$

$$r_{cr} = 0.3115 \quad c = 778.75$$

CHAPTER 5
FINITE ELEMENT METHOD MODEL

A nine node, non-conforming isoparametric plate finite element is employed for the damage theory implementation. The elements are based on Mindlin[19] deformation theory. Transverse shear deformations are allowed for in the formulation of this element. The motion of points not located on the mid-surface are governed by the rotations θ_x and θ_y , of lines that were perpendicular to the mid-plane of the undeformed element. Note that the present damage formulation does not modify the transverse stiffness of the elements.

5.1 FEM Formulation

The specimen was considered as an x-y plane model with the displacement in z direction. The thickness in z direction was so small for variation that we can ignore the effect. The plate constitutive law in equation(3.2) are used to shape the stiffness matrix for plane finite element model. The plate displacements include transverse deflection w and rotation angle θ_x and θ_y . The displacements components of the laminated plate are assumed to be of the form[20].

$$\begin{aligned} u(x, y, z) &= u^o(x, y) + z\phi_x(x, y) \\ v(x, y, z) &= v^o(x, y) + z\phi_y(x, y) \\ w(x, y, z) &= w^o(x, y) = w(x, y) \end{aligned} \tag{5.1}$$

where u^o , v^o and w^o are the mid plane displacement components in the x , y , z directions, respectively; and ϕ_x and ϕ_y are the rotations of cross-sections perpendicular to the x and y axes, respectively. We have assumed that u and v vary linearly in the thickness directions, while w is constant through the thickness.

The strain components for a point in the k th ply of the laminated plate z distance away from the mid plane can be computed as

$$\begin{aligned}\varepsilon_{xx}^k &= \varepsilon_x^o + z \kappa_x \\ \varepsilon_{yy}^k &= \varepsilon_y^o + z \kappa_y\end{aligned}\quad (5.2)$$

and shear strains are expressed as

$$\begin{aligned}\gamma_{xy}^k &= \gamma_{xy}^o + z \kappa_{xy} \\ \gamma_{yz}^k &= \frac{\partial w}{\partial y} + \frac{\partial v}{\partial z} = \frac{\partial w}{\partial y} + \phi_y = \gamma_y^o z \\ \gamma_{xz}^k &= \frac{\partial w}{\partial x} + \frac{\partial u}{\partial z} = \frac{\partial w}{\partial x} + \phi_x = \gamma_x^o z\end{aligned}\quad (5.3)$$

where

$$\begin{aligned}\varepsilon_x^o &= \frac{\partial u^o}{\partial x} \\ \varepsilon_y^o &= \frac{\partial v^o}{\partial y} \\ \gamma_{xy}^o &= \frac{\partial u^o}{\partial y} + \frac{\partial v^o}{\partial x}\end{aligned}\quad (5.4)$$

are the in-plane strain components of the mid plane

The rotation gradients are as follows.

$$\begin{aligned}\kappa_x &= \frac{\partial \phi_x}{\partial x} \\ \kappa_y &= \frac{\partial \phi_y}{\partial x} \\ \kappa_{xy} &= \frac{\partial \phi_x}{\partial y} + \frac{\partial \phi_y}{\partial x}\end{aligned}\quad (5.5)$$

Since w , ϕ_x , and ϕ_y are independent of z , it follows that the transverse shear strains are constant through the thickness of the plate.

The element displacement $[u]$ is derived from the multiplication of the shape function $[\Phi]$ with the nodal displacement $[\Delta]$.

$$[u] = [\Phi][\Delta] \quad (5.6)$$

Figure 5.1 illustrates the shape functions in natural coordinate.

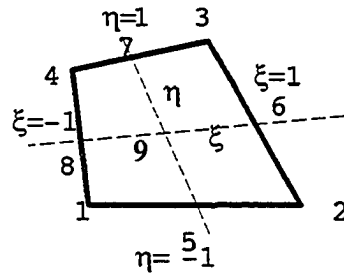


Figure 5.1 Nine Node Isoparametric Element

The shape functions for all nodes are as follows

for corner nodes ($\xi = \pm 1, \eta = \pm 1$)

$$s_i = \left(\frac{1}{4}\right)(1 + \xi_0)(1 + \eta_0)(\xi_0 + \eta_0 - 1) + \left(\frac{1}{4}\right)(1 - \xi^2)(1 - \eta^2) \quad (5.7)$$

for nodes at $\xi = 0$ and $\eta = \pm 1$

$$s_i = \left(\frac{1}{2}\right)(1 - \xi^2)(\eta_0 + \eta^2) \quad (5.8)$$

for nodes at $\xi = \pm 1$ and $\eta = 0$

$$s_i = \left(\frac{1}{2}\right)(\xi_0 + \xi^2)(1 - \eta^2) \quad (5.9)$$

for the center node

$$s_i = (1 - \xi^2)(1 - \eta^2) \quad (5.10)$$

In the shape functions above, ξ and η are local coordinates.

$$\xi_o = \xi \xi_i \quad \eta_o = \eta \eta_i \quad (5.11)$$

where ξ_i and η_i are natural coordinates of node i

Using the shape functions list above, the plate displacements are obtained by

$$[u]_{5 \times 1} = [\Phi]_{5 \times 45} [\Delta]_{45 \times 1} \quad (5.12)$$

where $[u]$ is the displacement vector, $[\Phi]$ is the matrix containing all shape functions, and $[\Delta]$ is a nodal displacement vector.

The mid plane strains and curvatures can be written in terms of the nodal displacements by performing the differentiation on equation(5.12).

$$\{\varepsilon\} = [B][u] \quad (5.13)$$

where $[B] = \partial [\Phi]$, $[u]$ is the element displacement .

Equations of motion of a laminated plate are obtained using a standard finite element procedure:

$$[M]\{\ddot{\Delta}\} + [K]\{\Delta\} = \{F\} \quad (5.14)$$

where $[M]$ is the mass matrix, $[K]$ is the stiffness matrix, and $\{F\}$ is the nodal force vector.

5.2 The FEM model

Wolfe [1] in his experiment chosen a simple-supported column as a specimen. In such a configuration, the stress state varies along the length when subjected to loads close to the buckling load. A gradient stress field in which maximum stress occur in the middle of the

specimen exists when columns lateral displacement is large. The specimen ends are fitted into slotted steel blocks; again a tight fit is ensured with brass and steel shims. The slots are made 25 mm deep, so the test section of the specimen between the end pieces is 37.5 mm by 150 mm. The total length of the column including the end pieces is 224 mm. These end pieces have a groove on the opposite surface into which the knife edge fit. The knife edges consist of blocks of 4041 steel, harden to 36 Rockwell, with one end machined down to a wedge with a rounded edge. A radius of 1.59 mm was chosen for the knife edge and the grooves in the end pieces. The blocks were then placed in the grips of the test machine[1]. After considering the effect of the interlaminar stress zone at the free edge and the effects of the thickness and the length on the column buckling load, a specimen of 200 mm in length and 37.5 mm in width is chosen. Laminates used in the experimental program resulted in thicknesses of approximately 7.5 to 8.6 mm.

A test jig was used with which to load the column with simply-supported boundary in his experiment. Friction problems with this jig were overcome by designing in an eccentricity to the load introduction points. The jig design in Wolfe experiment is illustrated in Figure 5.2.

The specimen geometry described above is modeled for the finite element analysis. Because of the number of plies in the specimens is too large, the coupling between twist and bending is neglectable. Therefore, a quarter part of the specimen is modeled. The FEM mesh for the quarter model is shown in Figure 5.3. 112 elements are used to model the quarter of the specimen. Finer mesh is generated near the centerline in x coordinate in order to get the precise result of strains and deflections. Boundary conditions for the FEM model are as follows. The nodes on centerline are allowed to move in y, z and θ_y coordinates. The nodes on the boundary(x=112 mm) on which the loads are applied, are allowed to move in x, y, θ_x and θ_y coordinates. The nodes on the x axis are allowed to move in x, z and θ_x coordinates. All other nodes have x, y, z, θ_x , and θ_y degrees of freedom.

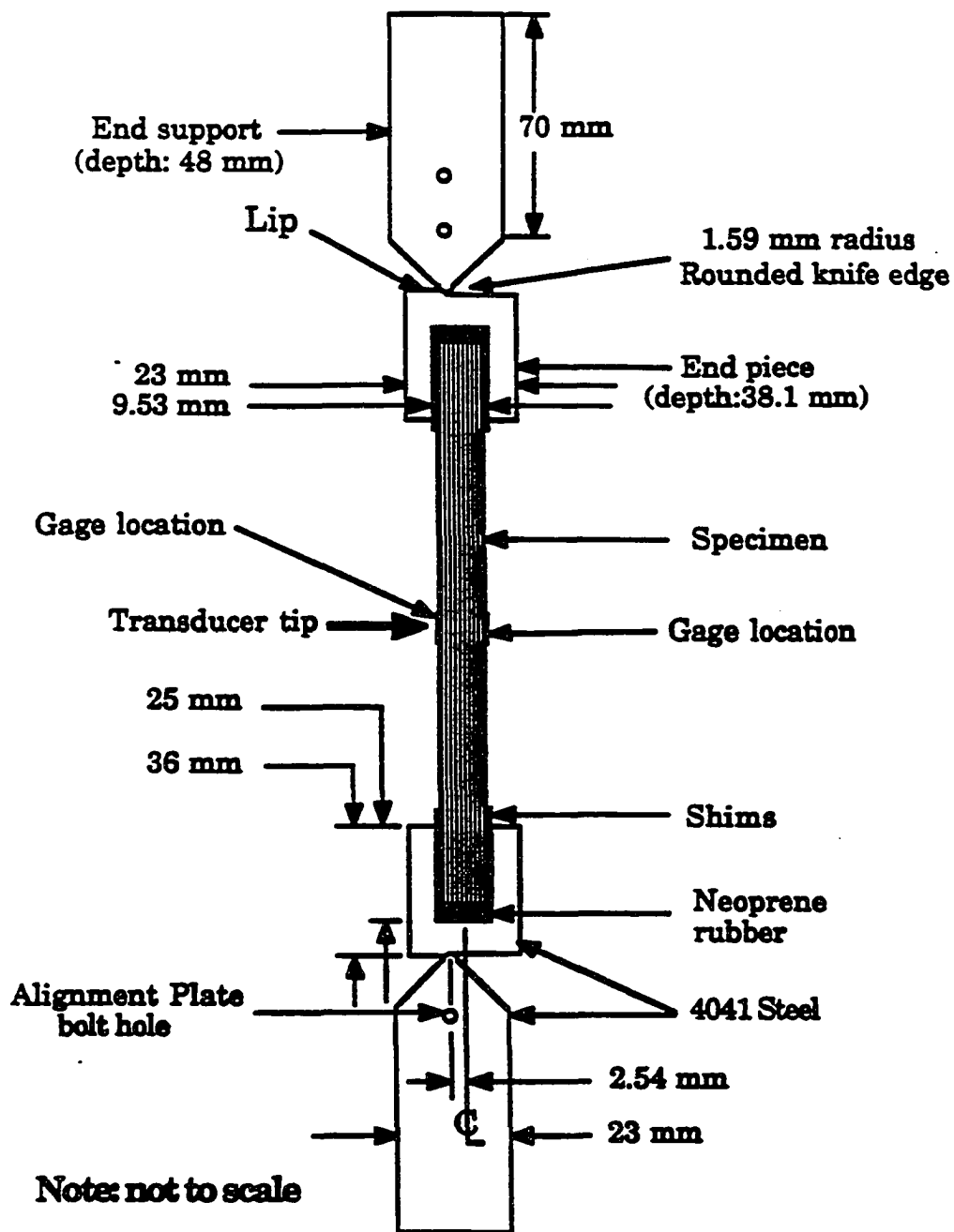


Figure 5.2 Configuration of Test Jig [1].

The compressive in-plane load and moment corresponding to the eccentricity of the load used by Wolfe[1] are applied at the edge($x=112$ mm). The consistent nodal loads and moments are calculated corresponding to the actual experimental loads.

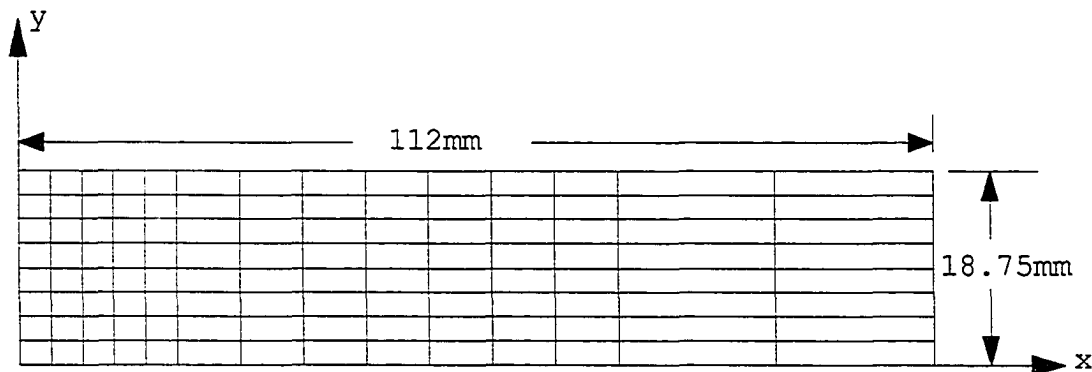
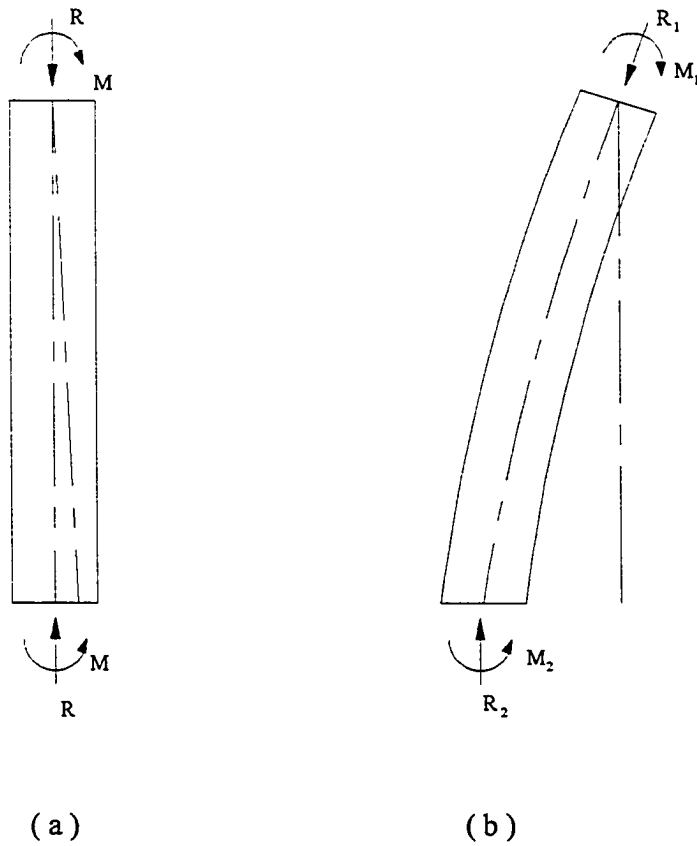


Fig 5.3 Mesh Generation in Laminate

5.3 FEM Procedure for Large Displacement

In structural mechanics, a problem is nonlinear if the stiffness matrix or the load vector depends on the structural deformation. The problem of structures with damage evolution are non-linear because the stiffness matrix is dependent on deformations. A column under eccentric compressive load results in a large lateral displacement. This makes the problem geometrically nonlinear because of large displacements. This section describes implementation of load vector modification due to large displacements in the finite element procedure.

Figure 5.4 shows equilibrium of a small element of a column under compressive in-plane load and moment for a small displacement and a large displacement configurations.



(a) (b)

Figure 5.4 Equilibrium of a Small Element of a Column
under Compressive in-plane Load and Moment

An approximate approach to implement the load vector modification due to large displacement is incorporated in the finite element procedure. The nodal moments are modified but the nodal loads are kept same as initial loads in the load vector. The equilibrium state of an element under the approximate approach implementation is shown in Figure 5.5.

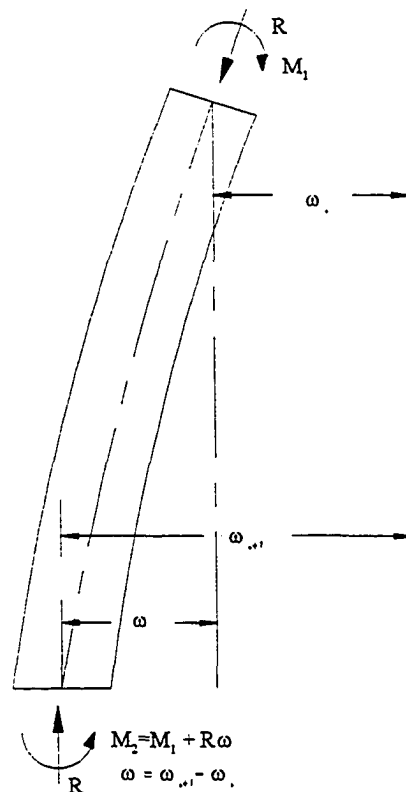


Figure 5.5 An Approximate Approach in Load Modification due to
Large Displacement

The nodal moments are modified at every load increment step. In addition, they are also modified during iterations within a loading step utilized for the damage convergence. At the first step, lateral displacement of nodes is zero and the initial load vector consists of in-plane compressive load and moment at the edge nodes (applied load) and the remaining nodal loads are identically zero. Nodal degrees of freedom (displacements and rotations) are obtained using the load vector and the current stiffness matrix. The difference in the lateral displacements of the successive nodes in the loading direction, obtained in the previous iteration, multiplied by the compressive edge nodal load is applied at successive nodes in the loading direction. These are moments applied to nodes by the deformed elements. (see Figure5.6)

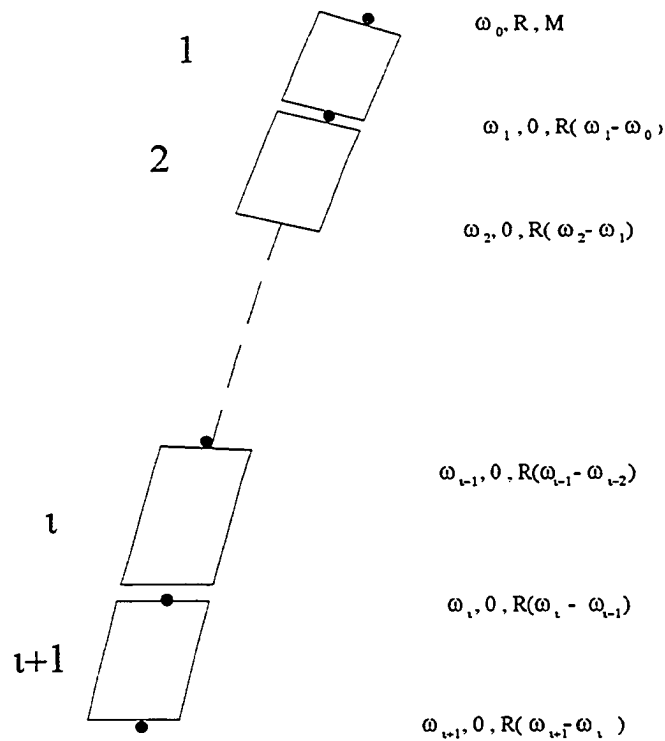


Figure 5.6 Relationship between Lateral Displacement, in-plane Load and Moment on Successive Nodes

It should be noted that the element equilibrium is approximately satisfied because nodal load and moment modification due to element rotation is not implemented in the numerical procedure.

5.4 Damage Evolution Model Implementation

Equation(3.15) depends on the damage parameter r in the formulation of the stiffness matrix. However, r itself is a function of the strain state, which in turn depends upon the stiffness matrix. Thus an iterative technique is required to evaluate the effect of damage growth on the stiffness of the structure.

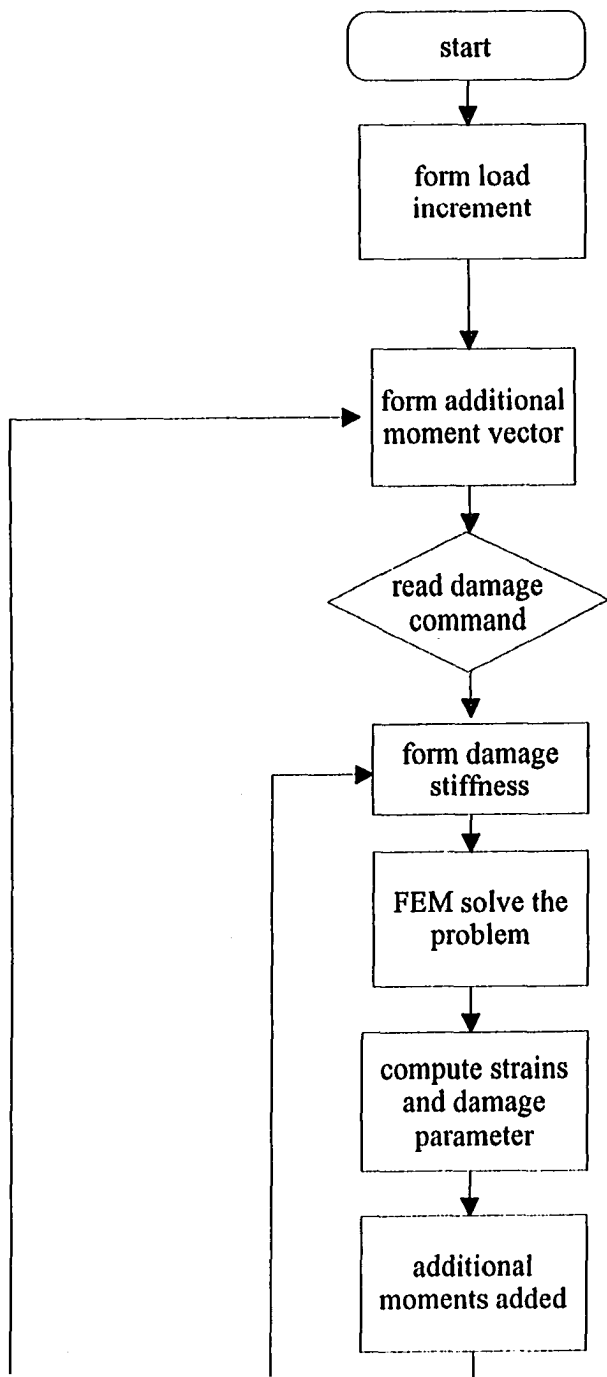
Initially, the material is assumed to consist wholly of undamaged material with tensile properties. A fraction of the external load is applied to the model and solved. This step determines the sense of the strains, either tensile or compression, a given ply carries. A per ply examination of the sense of the strains is performed, which reassigns the material properties of a given layer based upon the sense of the most critical principal strain component. This procedure is necessary due to the different damage growth behavior under tension and compression.

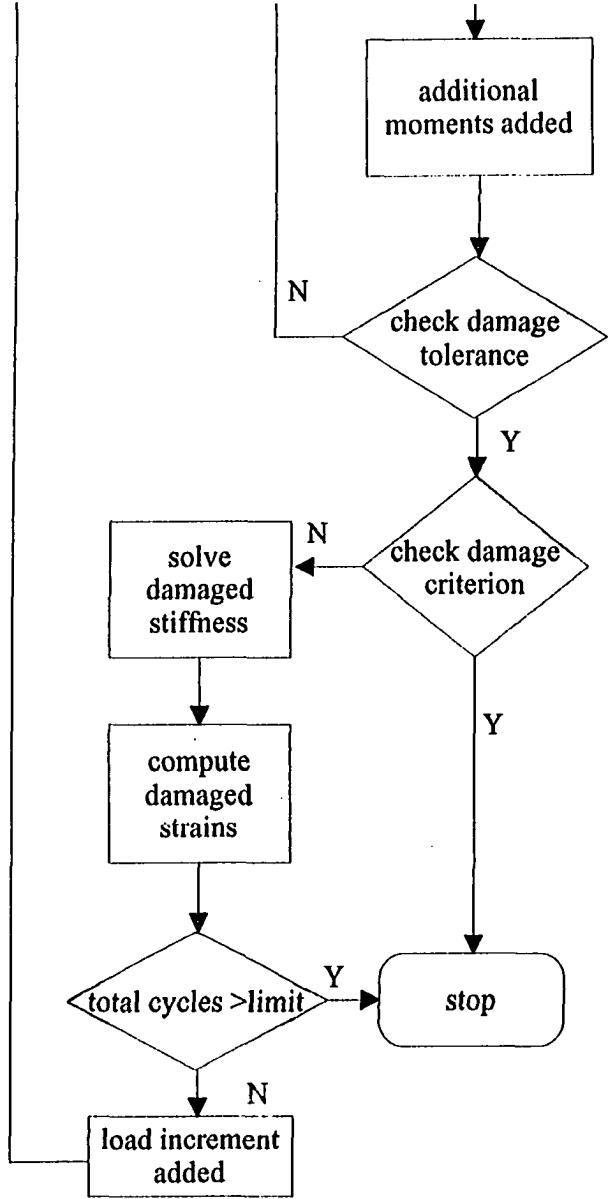
Once the material properties have been assigned, the applied loads are incremented in small steps. The number of increments is an input to the program. The FEM is solved for the initial load increment. The strain is stored, and equation(3.11) is employed to calculate an initial value of r for the current strains. This value of r is substituted back into equation(3.15) to form a modified stiffness matrix. Note that the value of r is stored, and renamed r_{prev} , and is employed later for convergence comparison. The FEM is again solved for the applied loads, but now with the updated stiffness matrix, which reflects the current values of r for each element on a ply-by-ply basis. The element strains again are used in equation(3.11) to calculate new value of r for the elements. The difference between the current value of r and r_{prev} for individual element plies is compared with a defined tolerance. The iterative process continues until all element plies in the model have converged to their particular values of r for the given load increment.

Once the values of r have converged, a comparison is made to evaluate whether r_{cr} has been attained. If so, the damage growth law and material properties of the pertinent ply are modified to reflect the dominant mode of the damage. Equation(3.18) or (3.19) describe either matrix degradation or fiber fracture damage growth. Additionally, a check is performed to examine whether the failure criteria of all the plies of an element attaining at least r_{cr} has been fulfilled.

This program code was run on a CRAY Y-MP8/864 system. Figure 5.7 shows the flowchart of the logic to implement the damage theory and load modification numerically into finite element.

Figure 5.7 Flowchart for Damage Evolution Model Implementation





CHAPTER 6

NUMERICAL SIMULATIONS

The experimental response of laminated composite columns under eccentric compressive load is numerically simulated. Wolfe[1] used classical lamination plate theory and the maximum stress failure criterion to choose two laminates such that initial damage would occur in the 90 plies and one such that damage would initially occur in the 45 plies, all on the tension side. As mentioned in the previous chapter, the first two lay-ups are $[\pm 45^\circ / 0^\circ / 90^\circ]_{4s}$ and $[(45^\circ_2 / -45^\circ_2 / 0^\circ) / 90^\circ]_{2s}$. The last lay-up is $[-45^\circ_4 / -45^\circ_4 / (0^\circ / 90^\circ)_4]_{2s}$.

The nominal length of specimens with end pieces (see Figure 5.2) is 224 mm. The effective length of specimens free to bend is 150 mm. The numerical simulation considered the total length of the specimens free to bend. This assumption in the numerical simulations results in more deformation than the experimental constrained specimens deformation.

Table 6.1 compares maximum load, first ply damage and subsequent damage from experimental and numerical results. In the $[-45^\circ_4 / -45^\circ_4 / (0^\circ / 90^\circ)_4]_{2s}$ specimen, the model prediction of maximum load (14400 N) is above the experimental range (10278-12343 N). The numerical prediction of the ply in which first critical damage occurs is same as experimental result that the damage initiates in ± 45 outermost tension side group of plies. The center deflection obtained from the numerical analysis is almost the same as the experimentally observed deflection, however, the damage initiation load from the analysis (11640 N) is higher than the experimental result by 5%. The prediction of the ply in which the subsequent damage occurs is exactly the same as the damage initiation layers in the experiment. The subsequent load prediction by analysis (13200 N) is lower than the experimental result (14185 N) and the corresponding center deflection (14.5 mm) is higher than the experimental result (13.3 mm).

In the $[\pm 45^\circ / 0^\circ / 90^\circ]_{4s}$ specimen, the model prediction of maximum load (8400 N) is above the experimental range (6170-7624 N). The numerical prediction of the ply in which first critical damage occurs is same as experimental result that the damage initiates in 90 outermost tension side group of plies. The center deflection obtained from the numerical analysis is the same as the experimentally observed deflection, however, the damage initiation load from the analysis (7710 N) is higher than the experimental result by 8%. The prediction of the ply in which the subsequent damage occurs is exactly the same as the damage initiation layers in the experiment. The subsequent load prediction by analysis (8200 N) is lower than the experimental result (8754 N) and the corresponding center deflection (13.5 mm) is also lower than the experimental result (19.6 mm).

In the $[(45^\circ_2 / -45^\circ_2 / 0^\circ) / 90^\circ]_{2s}$ specimen, the model prediction of maximum load (10200 N) is above the experimental range (7455-9497 N). The numerical prediction of the ply in which first critical damage occurs is same as experimental result that the damage initiates in 90 outermost tension side group of plies. The center deflection obtained from the numerical analysis is the same as the experimentally observed deflection, however, the damage initiation load from the analysis (8820 N) is higher than the experimental result by 8%. The prediction of the ply in which the subsequent damage occurs is exactly the same as the damage initiation layers in the experiment. The subsequent load prediction by analysis (9800 N) is lower than the experimental result (10671 N) and the corresponding center deflection (15.2 mm) is also lower than the experimental result (15.7 mm).

Figure 6.1 shows center deflection as a function of applied compressive load for $[45^\circ_4 / -45^\circ_4 / (0^\circ / 90^\circ)_4]_{2s}$ laminated composite columns. The experimental curve is for a typical specimen. The numerical results are within experimental bounds. Both curves are plotted up to the first critical failure in respective cases. The strain on surface at the center of

the specimen are plotted in Figure 6.2. The model predicts higher strains up to the first critical failure. This is consistent with higher displacement predictions as shown in the Figure 6.1.

The consistent higher displacement and strain predications may be primarily attributed to neglecting constraint on bending due to the end caps which cover 37 mm of the specimen on both ends. The total specimen length is 212 mm. Similar plots for $[\pm 45^\circ / 0^\circ / 90^\circ]_{4s}$ and $[(45^\circ_2 / -45^\circ_2 / 0^\circ)_2 / 90^\circ_2]_{2s}$ are shown in Figure 6.3, Figure 6.4, Figure 6.5 and Figure 6.6 respectively.

Figure 6.7 (a) shows first damage along the longitudinal cross section of a typical $[45^\circ_4 / -45^\circ_4 / (0^\circ / 90^\circ)_4]_{2s}$ specimen. The first damage occurs in the outermost ± 45 group on the tension side. It should be noted that the position of the matrix crack in a longitudinal section depends on where the crack originates along the width direction. This is because the crack extends in 45 direction. The density plot of damage parameter in all the plies at the same longitudinal cross section is shown in Figure 6.7 (b). The density plot of the damage parameter is shown at the load level where first critical damage occurs in the ± 45 group. The darker gray scale represents higher level of damage. It is clearly seen that the tension side shows more damage than the compressive side. The damage in the outermost $[-45_4 / 45_4]$ ply group is shown in Figure 6.7 (c). The gray scale for the density plot is normalized in narrow range to show damage variation within the plies. Similar comparison of experimental observations of damage in the laminate when damage occurs in inner $[-45_4 / 45_4]$ ply group is shown in Figure (6.10). It is interesting to note that the cracks appear in groups at locations which can be identified as high damage locations from Figure 6.10 (c).

Table 6.1 Experimental Damage Initiation Loads and Model Predictions

specimen	maximum load		* occurrence of the first ply damage						occurrence of the subsequent damage					
			experiment			model			experiment			model		
	experiment (N)	model (N)	ply No. angle	load (N)	center deflection (mm)	ply No. angle	load (N)	center deflection (mm)	ply No. angle	load (N)	center deflection (mm)	ply No. angle	load (N)	center deflection (mm)
1	Max:12343 Min:10278 Av. :11372	14400	1-8 ±45	11065	9.83	1-8 ±45	11640	9.8	17-24 ±45	14185	13.3	17-24 ±45	13200	14.5
2	Max: 7624 Min: 6170 Av. :7085	8400	4-7 90	7132	11.6	4-7 90	7710	11.6	11-14 90	8754	19.6	11-14 90	8200	13.5
3	Max: 9497 Min: 7455 Av. :8431	10200	11-15 90	8115	9.84	11-15 90	8820	9.8	11-15 90	10671	15.7	11-15 90	9800	15.2
Remark	<p>1. * Experimental results are for a typical specimen.</p> <p>2. specimen 1 layup :$[45; / -45; / (0^{\circ} / 90^{\circ})]_{1,1}$</p> <p>3. specimen 2 layup :$[\pm 45^{\circ} / 0^{\circ} / 90^{\circ}]_{1,1}$</p> <p>4. specimen 3 layup :$[(45; / -45; / 0^{\circ}) / 90^{\circ}]_{1,1}$</p>													

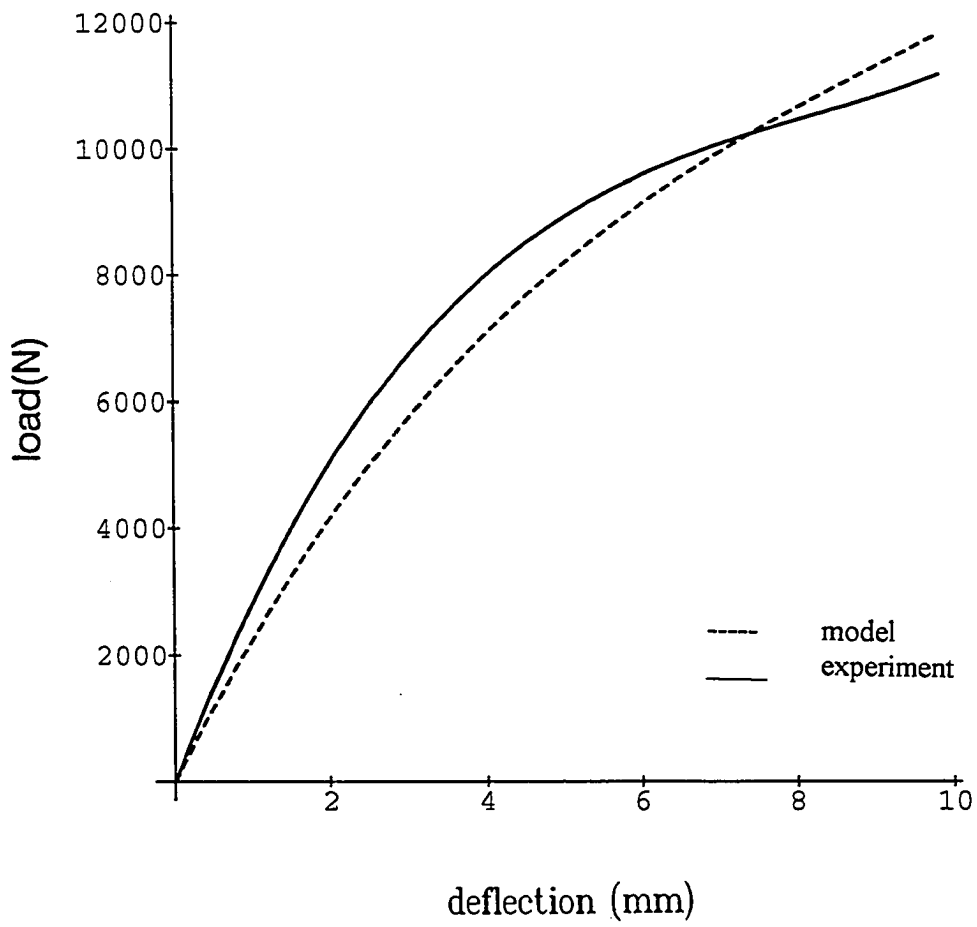


Fig 6.1 Experimental and Predicted Load versus Center Deflection for $[45_4 / -45_4 / (0^\circ / 90^\circ)_4]_{2s}$ prior to Damage

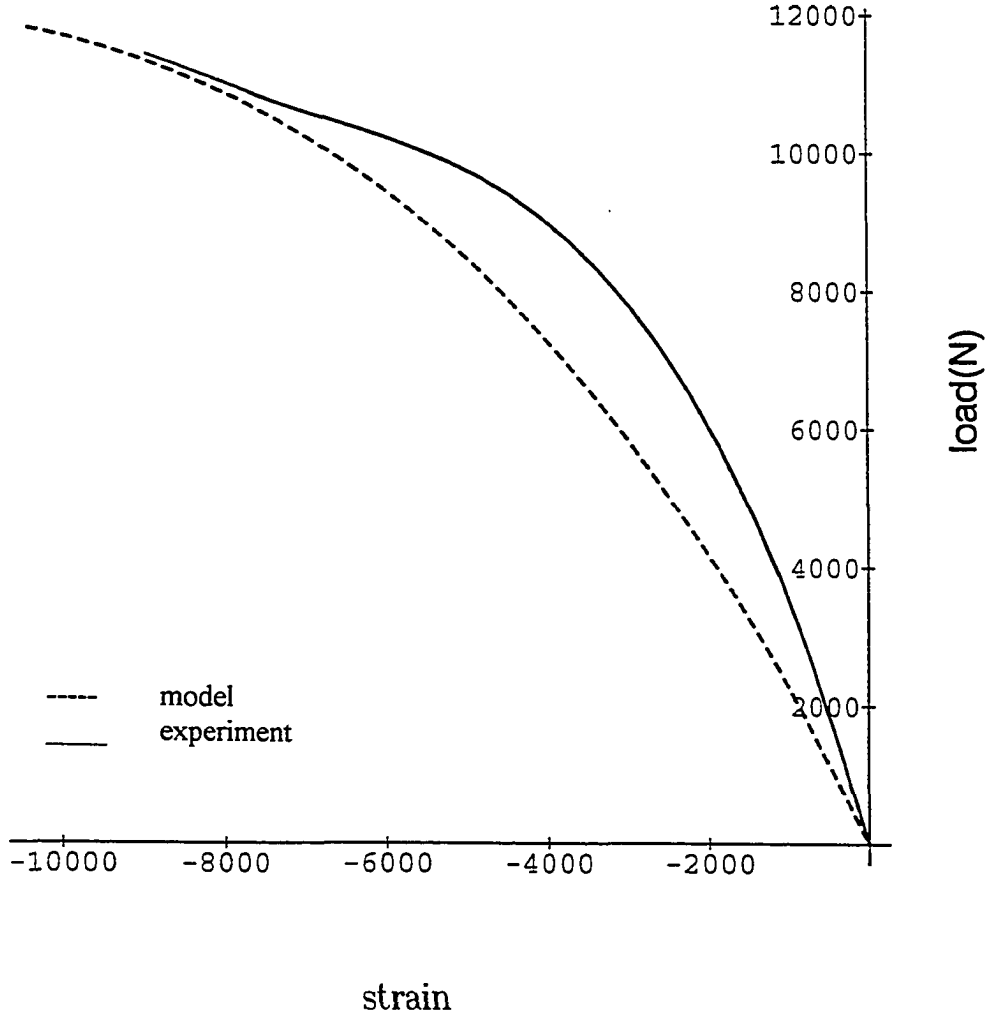


Fig 6.2 Experimental and Predicted Load versus Centerline Strain for $[+45^{\circ} / -45^{\circ} / (0^{\circ} / 90^{\circ})_4]_{2s}$ prior to Damage

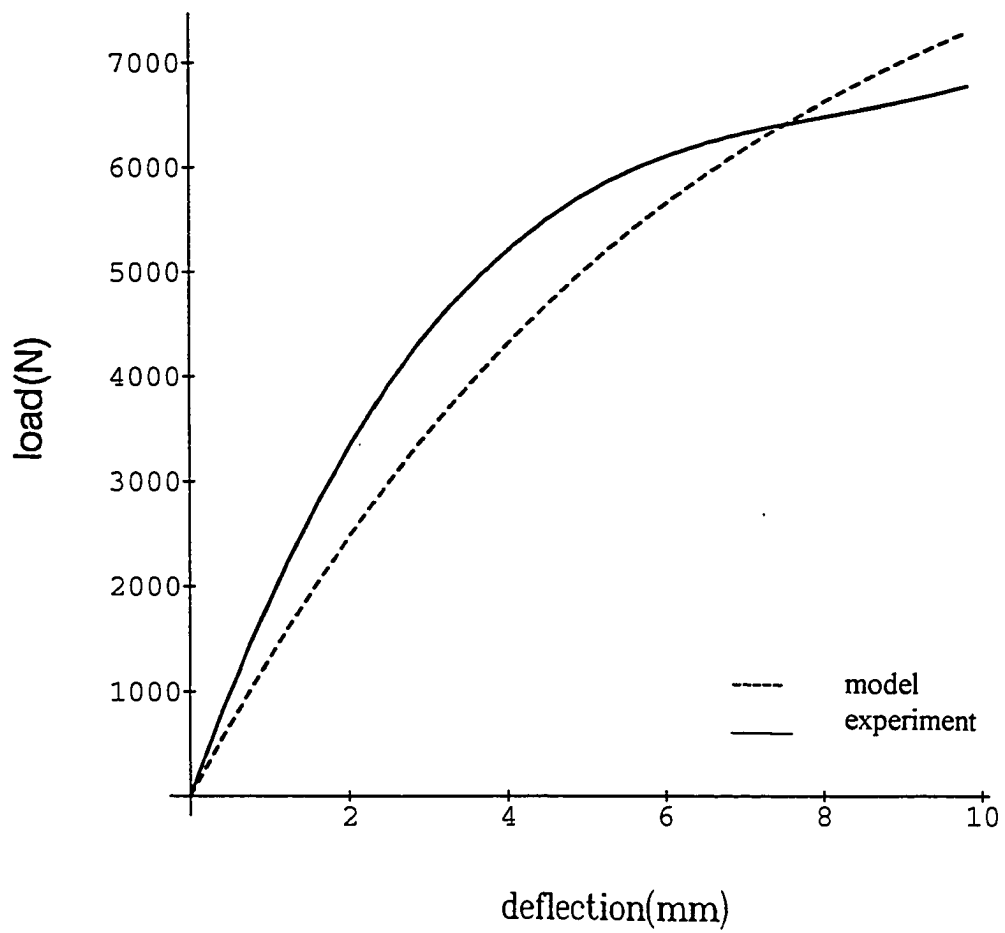


Fig 6.3 Experimental and Predicted Load versus Center Deflection for $[\pm 45^\circ / 0^\circ / 90^\circ]_{4s}$ prior to Damage

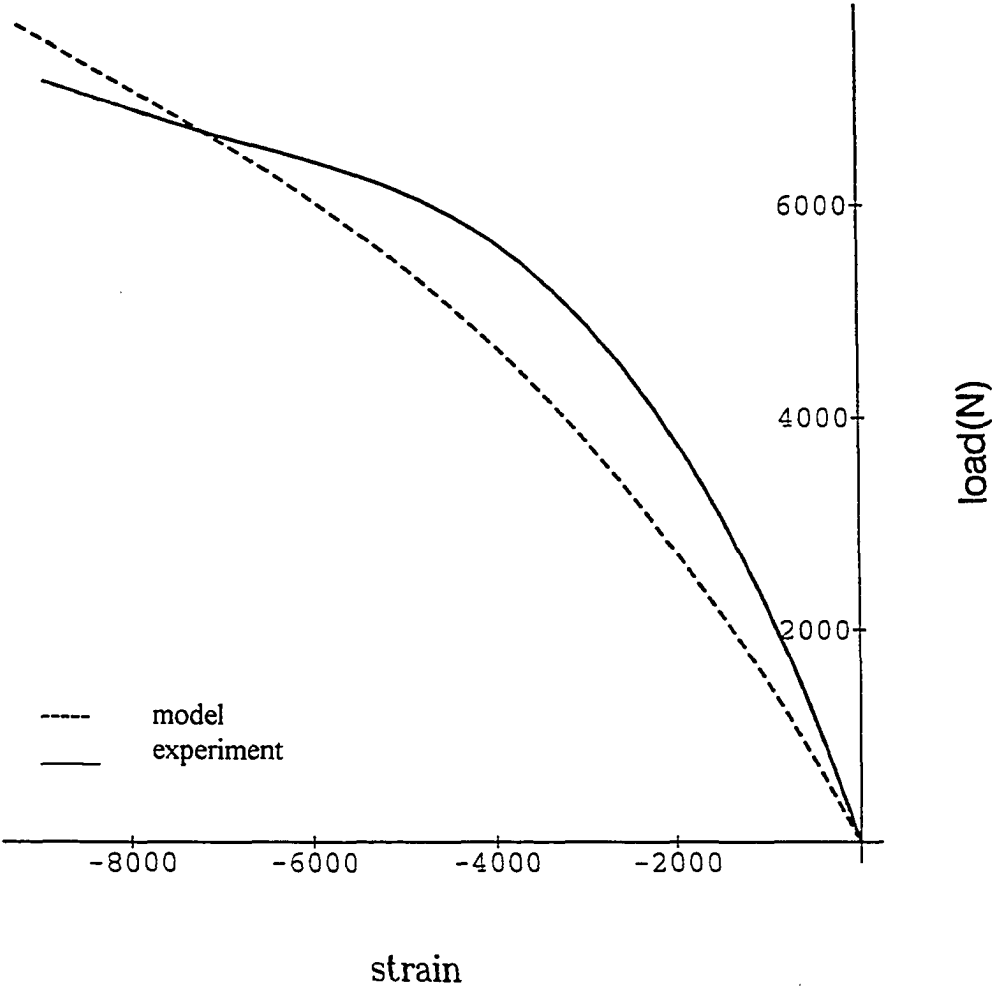


Fig 6.4 Experimental and Predicted Load versus Centerline Strain for $[\pm 45^\circ / 0^\circ / 90^\circ]_{s,s}$ prior to Damage

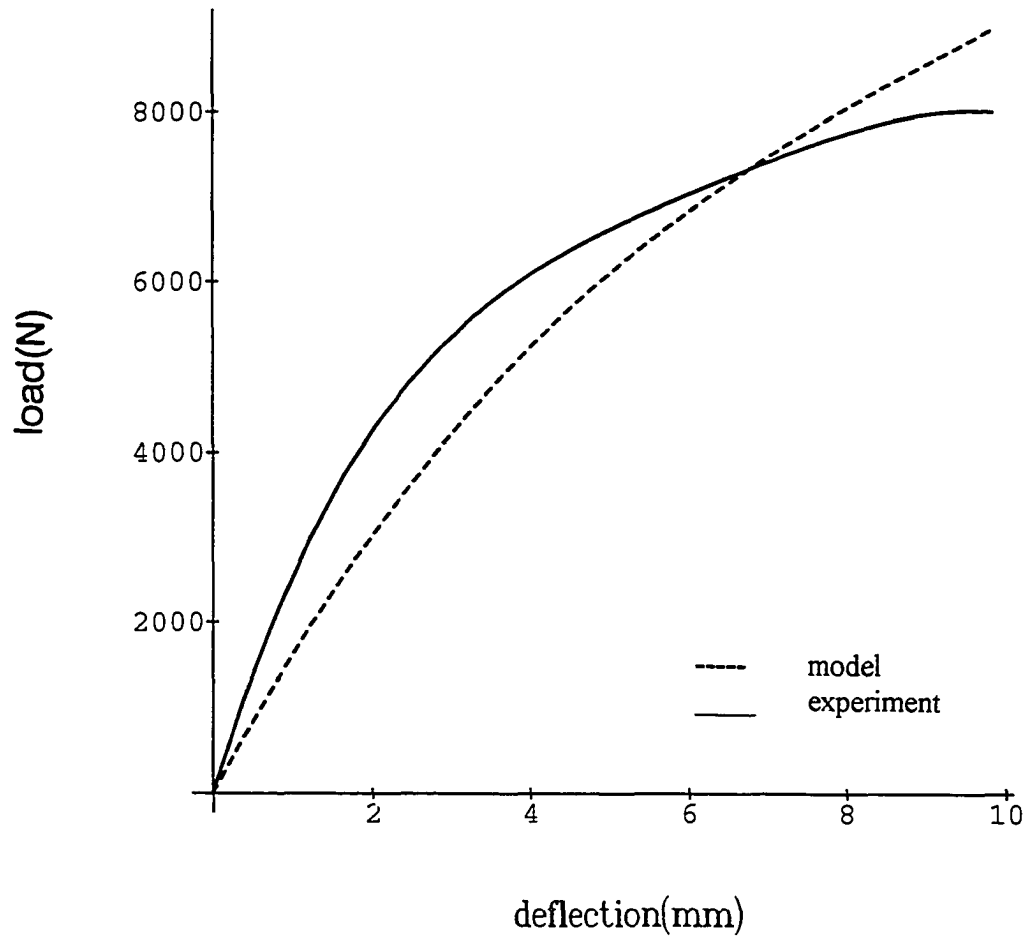


Fig 6.5 Experimental and Predicted Load versus Center Deflection for $[(+45_2 / -45_2 / 0^\circ)_2 / 90_2]_{2s}$ prior to Damage

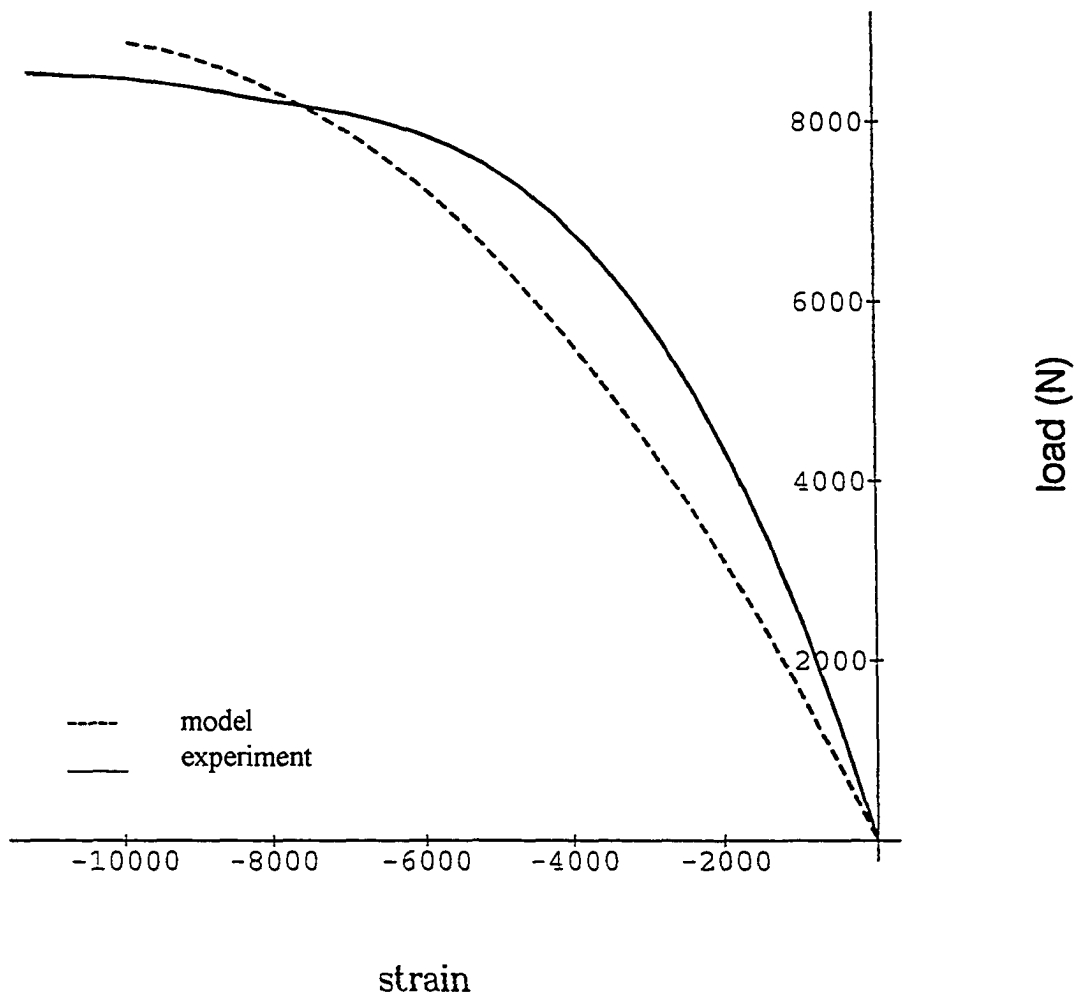
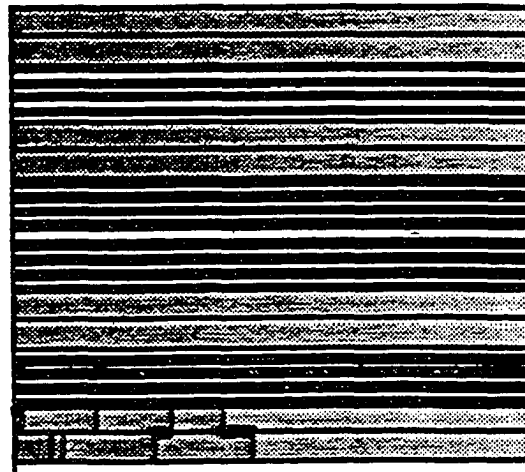


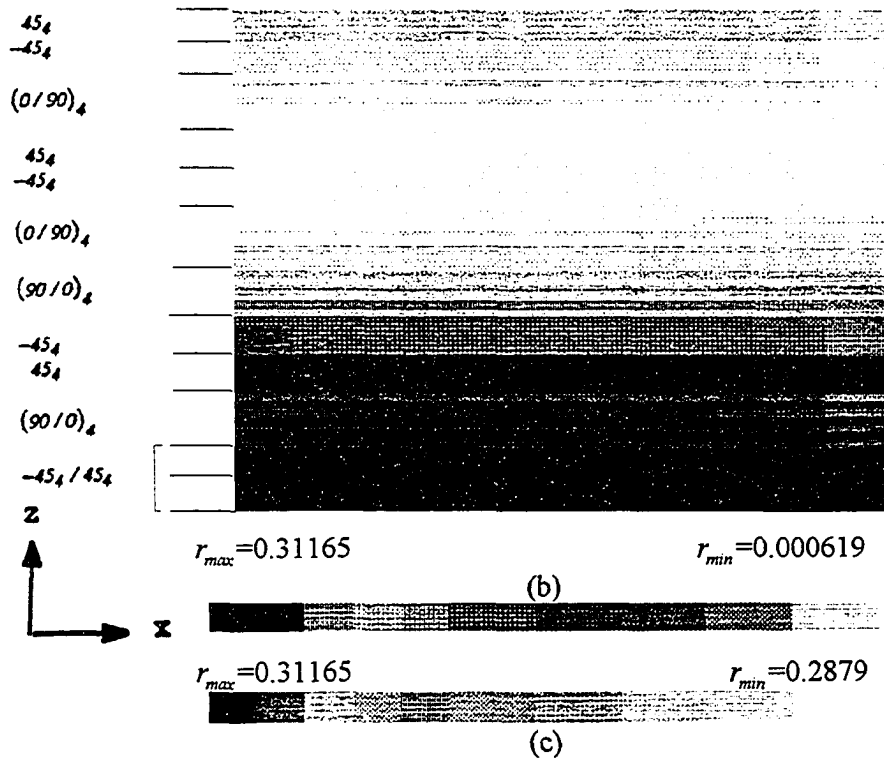
Fig 6.6 Experimental and Predicted Load versus Centerline Strain for $[(+45_2 / -45_2 / 0^\circ)_2 / 90_3]_{2s}$ prior to Damage

Figure 6.8 (a) shows first damage along the longitudinal cross section of a typical $[\pm 45^\circ / 0^\circ / 90^\circ]_{4s}$ specimen. The first damage occurs in the outermost 90 group on the tension side. It should be noted that the position of the matrix crack in a longitudinal section depends on where the crack originates along the width direction. This is because the crack extends in 90 direction. The density plot of damage parameter in all the plies at the same longitudinal cross section is shown in Figure 6.8 (b). The density plot of the damage parameter is shown at the load level where first critical damage occurs in the 90 group. The darker gray scale represents higher level of damage. It is clearly seen that the tension side shows more damage than the compressive side. The damage in the outermost 90 ply group is shown in Figure 6.8 (c). The gray scale for the density plot is normalized in narrow range to show damage variation within the plies. Similar comparison of experimental observations of damage in the laminate when damage occurs in inner 90 ply group is shown in Figure 6.11. It is interesting to note that the cracks appear in groups at locations which can be identified as high damage locations from Figure 6.11 (c).

Figure 6.9 (a) shows first damage along the longitudinal cross section of a typical $[(45^\circ_2 / -45^\circ_2 / 0^\circ)_2 / 90^\circ_5]_{2s}$ specimen. The first damage occurs in the outermost 90 group on the tension side. It should be noted that the position of the matrix crack in a longitudinal section depends on where the crack originates along the width direction. This is because the crack extends in 90 direction. The density plot of damage parameter in all the plies at the same longitudinal cross section is shown in Figure 6.9 (b). The density plot of the damage parameter is shown at the load level where first critical damage occurs in the 90 group. The darker gray scale represents higher level of damage. It is clearly seen that the tension side shows more damage than the compressive side. The damage in the outermost 90 ply group is shown in Figure 6.9 (c). The gray scale for the density plot is normalized in narrow range to show damage variation within the plies.



(a)



$$r_{max}=0.31102 \quad r_{min}=0.2767$$

Figure 6.7 First Critical Damage in $[45^\circ / -45^\circ / (0^\circ / 90^\circ)]_{2s}$ Lay-up.

- (a) Experimental Observed Matrix in Cross-section, $y=17.25$ mm, $x=30$ mm to 100 mm, at 11065 N Load. (b) Density Plot of Damage Parameter in the Same Cross-Section. (c) Enlarged Damage Parameter Density Plot in the -45,45 Layers.

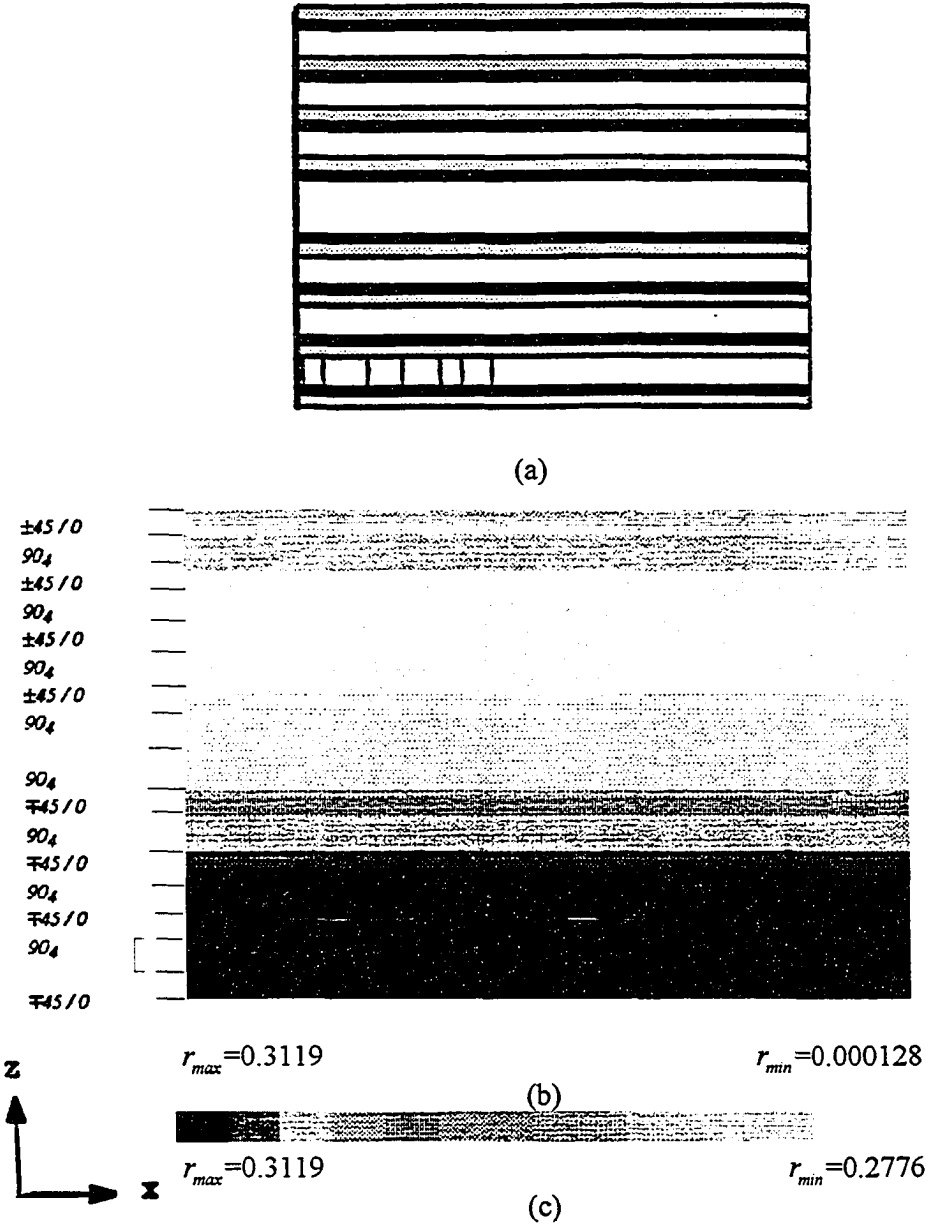


Figure 6.8 First Critical Damage in $[\pm 45^\circ / 0^\circ / 90^\circ]_s$ Lay-up.

- (a) Experimental Observed Matrix in Cross-section, $y=17.25$ mm, $x=30$ mm to 100 mm, at 7132 N Load.
- (b) Density Plot of Damage Parameter in the Same Cross-Section.
- (c) Enlarged Damage Parameter Density Plot in the 90 Layers.

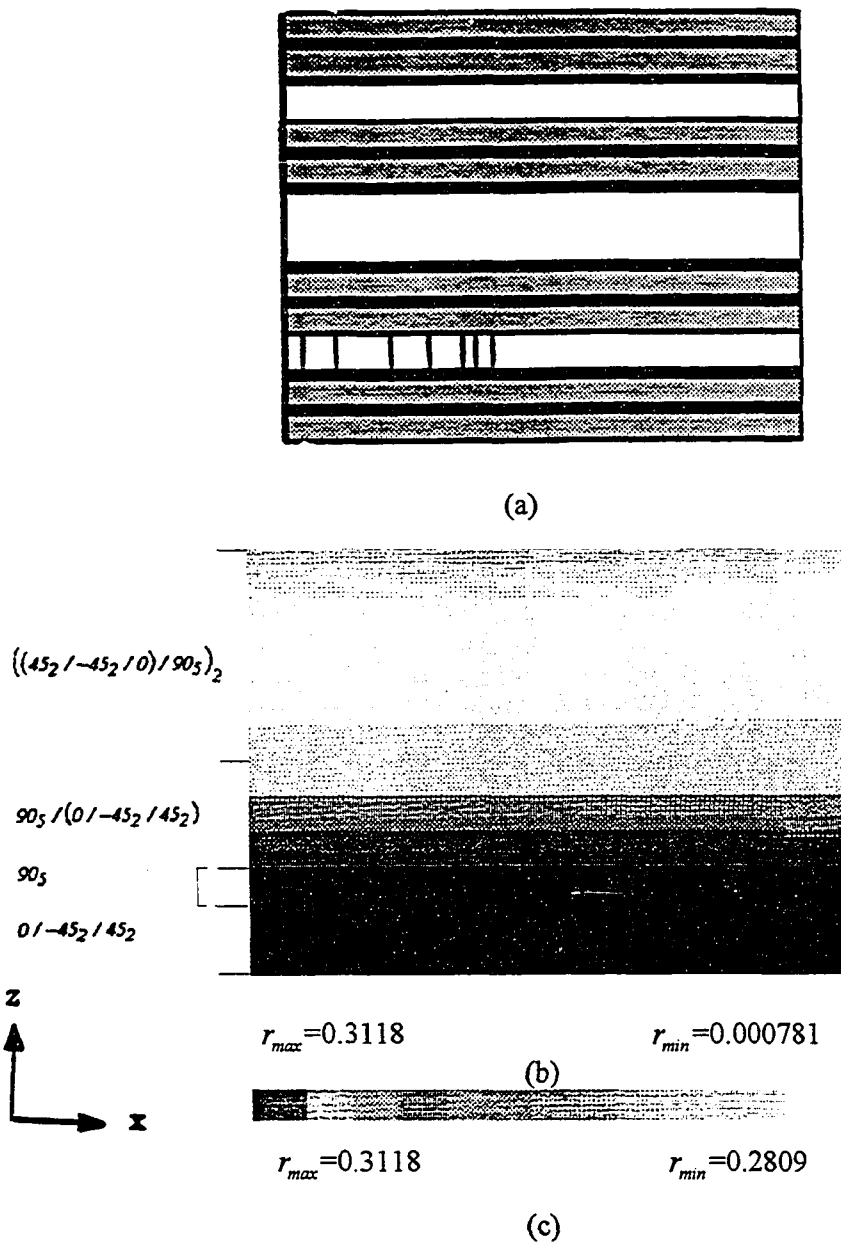


Figure 6.9 First Critical Damage in $[(45_2 / -45_2 / 0)_2 / 90_5]_{2s}$ Lay-up.

- (a) Experimental Observed Matrix in Cross-section, $y=17.25$ mm, $x=30$ mm to 100 mm, at 8115 N Load. (b) Density Plot of Damage Parameter in the Same Cross-Section. (c) Enlarged Damage Parameter Density Plot in the 90 Layers.

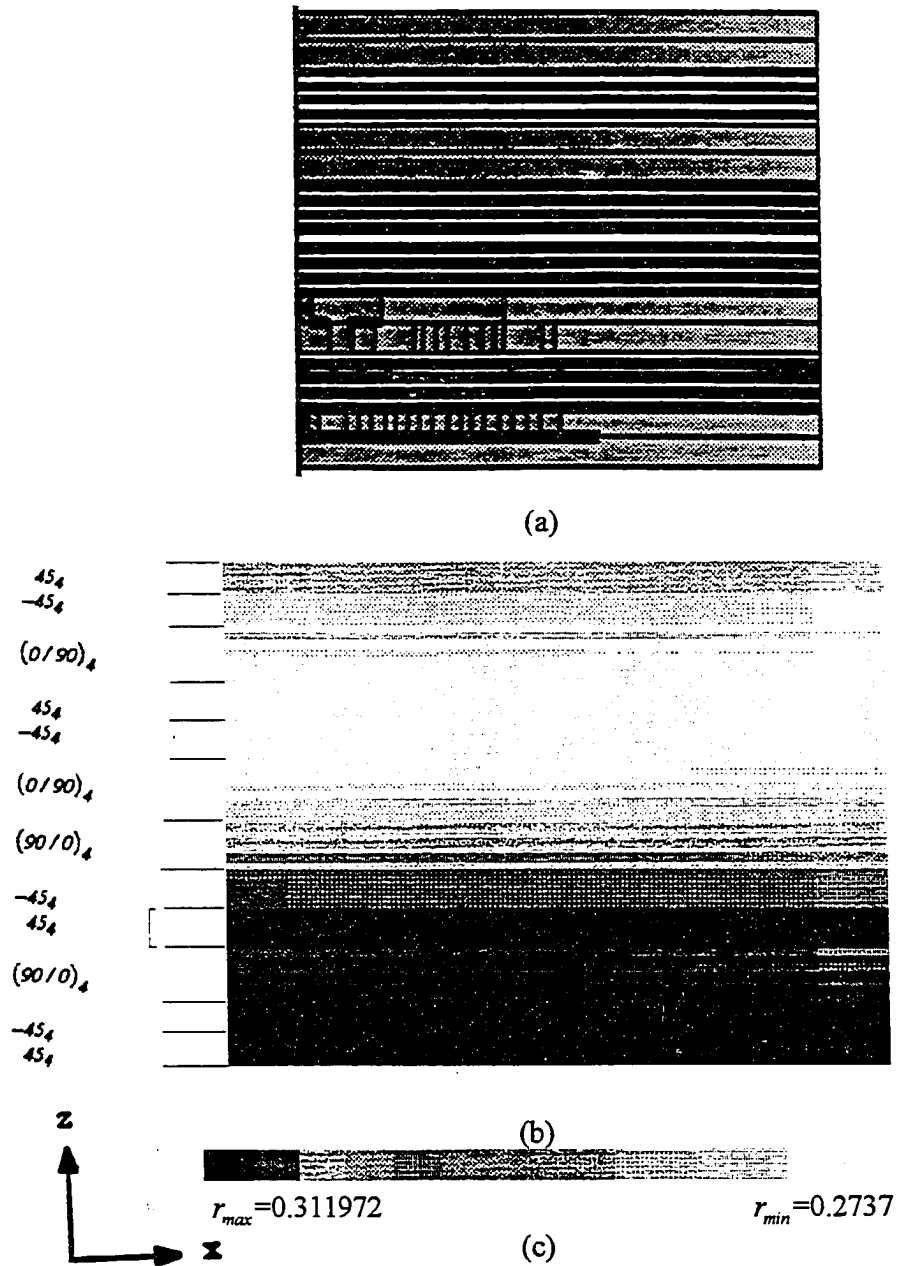


Figure 6.10 Subsequent Critical Damage in $[45^{\circ}_4 / -45^{\circ}_4 / (0^{\circ} / 90^{\circ})_4]_{2s}$ Lay-up.
 (a) Experimental Observed Matrix in Cross-section, $y=17.25$ mm, $x=30$ mm to 100 mm, at 14185 N Load. (b) Density Plot of Damage Parameter in the Same Cross-Section.
 (c) Enlarged Damage Parameter Density Plot in the 45 Layers.

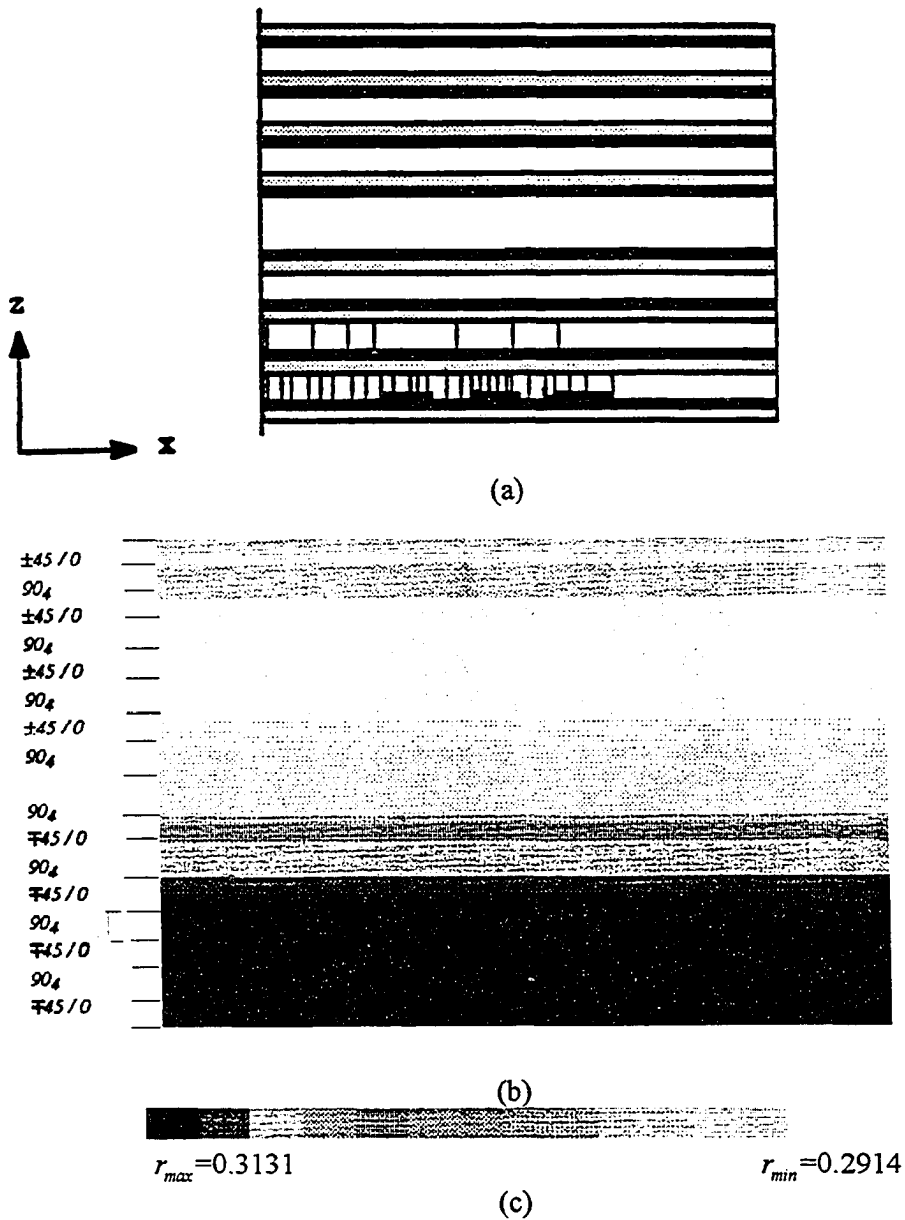


Figure 6.11 Subsequent Critical Damage in $[\pm 45^\circ / 0^\circ / 90^\circ]_s$ Lay-up.
 (a) Experimental Observed Matrix in Cross-section, $y=17.25$ mm, $x=30$ mm to 100 mm, at 8754 N Load. (b) Density Plot of Damage Parameter in the Same Cross-Section.
 (c) Enlarged Damage Parameter Density Plot in the 90 Layers.

CHAPTER 7

SUMMARY AND RECOMMENDATIONS

The two phases continuum damage theory is incorporated in a plate finite element procedure. The finite element program is capable of capturing damage evolution in each layer of every finite element. The FEM program is utilized to study the damage evolution in laminated composite plates. The gradient stress field in the plate is created with the application of in-plane compressive loads and moments. The out-of-plane displacement caused by the combination of compressive loads and edge moments produces in-plane shear gradients as well as through-the-thickness shear gradients.

The modeling of the experimental conditions[1] is not accurate. The end caps on specimens are ignored in the numerical analysis. The load modification due to the large displacement is approximately implemented. The nonlinear behavior of the specimens is primarily due to the large displacements. The critical damage in plies occurs with in 10% of the buckling load. In spite of the approximate implementation of the experimental conditions, the damage evolution predictions are close to the experimental observations.

The following recommendation are made on the basis of the limitation of the present FEM procedure and the two phase continuum damage theory.

- (1) The FEM code should be optimized to fully take advantage of vector processing capabilities of the computer CRAY Y-MP8/864 system. The code is currently running CRAY Y-MP8/864 system and typically takes 45 minutes of C.P.U. time.
- (2) The two phase continuum damage model should be improved to take into account free-edge stress and delamination.

(3) The geometric nonlinearity due to large deflections should be implemented accurately in the model.

(4) The two phase continuum damage model should also be improved to incorporate the effect of transverse shear in damage progression.

REFERENCES

1. Wolfe, C.E., "Damage Accumulation in a Gradient Stress Field in Graphite/Epoxy Laminates , " M.I.T.Master's Thesis, 1989.
2. Leissa, A.W., "Buckling of Laminated Composite Plates and Shell Panels, " Technical Report AFWAL-TR-85-3069, 1985.
3. Minguet, P.J. , Dugundji, J. and Lagace, P.A. , "Post buckling Behavior of Laminated Plates Using Direct Energy Minimization Technique, " *AIAA Journal* ,Vol. 27, No 12, December 1989.
4. Jensen, D.W. and Lagace, P.A. , "Influence of Mechanical Couplings on the Buckling and Post-Buckling of Anisotropic Plates, " *AIAA Journal* ,Vol.26, No 10, October 1988.
5. Kachanov , L.M. , "On the Creep Fracture Time," *Izvestia AN SSR , Otd. Tekhn. Nauk*; No. 8, 26-31(1958).
6. Onsager, L. , "Reciprocal Relation in Invisible Process I., " *Physics Review* Vol.37, 1931, 405-426(1931).
7. Goode, R.J., "A Finite Element Implementation of a Deformation Based Continuum Damage Mechanical Model, " The University of Texas at Arlington Master's Thesis, 1991.
8. Reifsnider, K.L. , Henneke, E.G. and Stinchcomb, W.W. , "The Mechanics of Vibrothermography," In *Mechanics of Nondestructive Testing*, ed. W.W. Stinchcomb. Plenum Press, New York, 1980.
9. Stinchcomb, W.W. , "Nondestructive Evaluation of Damage Accumulation Precesses in Composite Laminates," *Comp. Science and Tech.* , 25 (1986), 103-118(1986).

10. Tsai, S.W. , "Strength Theories of Filamentary Structures," In *Fundamental Aspects of Fiber Reinforced Plastic Composite*, ed. R.T. Schwartz and H.S. Schwartz. Wiley, New York, 3-11(1968).
11. Schapery, R.A., "On Viscoelastic Deformation and Failure Behavior of Composites Materials with Distributed Flaws," *Advances in Aerospace Structures and Materials*, ASME, AD-01, 5-20(1981).
12. Laws, N., Drorak, G.J. and Hejazi,M., "Stiffness Changes in Unidirectional Composites Caused by Crack Systems, " *Mech. of Materials*, 2 , 194-218(1983).
13. Talreja, R."A Continuum Mechanics Characterization of Damage in Composites, " *Proc. Roy. Soc. London*, 399, 195-216(1985).
14. Allen, D.H., Harris, C.E. and Groves, S.E., " A Thermomechanical Constitutive Theory for Elastic Composites with Distributed Damage: I. Theoretical Development," *Intl. J. Solids Struc.* 23, 1301-1318(1987).
15. Allen, D.H., Harris, C.E. and Groves, S.E., " A Thermomechanical Constitutive Theory for Elastic Composites with Distributed Damage : II. Application to Matrix Cracking in Laminated Composites," *Intl J. Solids Struc.* 23, 1319-1338(1987).
16. Frantziskonis, G., "Distributed Damage in Composites, Theory and Verification, " *Composite Structure* 10, 165-184(1988).
17. Frantziskonis, G., and Joshi, S.P., "Damage Evolution and Constitutive Behavior of Advanced Composites, " *Comp. Struct. Intl. Journal* 16, 341-357(1990).
18. Joshi, S.P. and Frantziskonis , G.,, "Damage Evolution in Laminated Advanced Composites," *Comp. Struct. Intl. Journal* 17,127-139(1990).
19. Cook, R.D., Malkus, D.S. and Plesha, M.E.,*Concepts and Applications of Finite Element Analysis*, John Wiley & Sons, New York,1989.
20. Yang, P.C., C.H. Norris, and Y. Starsky, "Elastic Wave Propagation in Heterogeneous Plates," *Intl. J. Solids and Struc.*2,665-683(1966).